

# COMPUTATIONAL MODELING OF STRAND-BASED WOOD COMPOSITES

By Peggi L. Clouston,<sup>1</sup> P.E., and Frank Lam,<sup>2</sup> P.E., Member, ASCE

**ABSTRACT:** A nonlinear stochastic model has been formulated to simulate the stress-strain behavior of strand-based wood composites based on the constitutive properties of the wood strands. Prediction models of this type save time and money in the development of wood composites by computationally gauging the effects of varying raw material characteristics with limited fabrication and testing of the full-scale product. The proposed model uses a stochastic-based materially nonlinear finite-element code with extended capacity to perform Monte Carlo simulations to predict the stress-strain behavior of  $[\pm 15]$ , and  $[\pm 30]$ , angle-ply laminates in tension and compression. The nonlinear constitutive behavior of the wood strands is characterized within the framework of rate-independent theory of orthotropic plasticity, where the plastic flow rule is in accordance with the Tsai-Wu criterion. Shear strength and stiffness of the strands, as well as the interaction parameter of the Tsai-Wu criterion have been estimated through a minimization technique developed in the present study. The model's accuracy was validated through comparisons of the numerical simulation results and experimental data. Excellent agreement was found.

## INTRODUCTION

The development of structural composite lumber (SCL) [e.g., Parallel Strand Lumber (PSL) and Laminated Strand Lumber (LSL)] has depended predominantly upon expensive empirical-based research initiatives. The products were gradually refined through experimental manipulation of the constituents to what we know today as viable building materials. The process was costly and time consuming. The development could have been hastened significantly, however, with the aid of a computational model. Computer models can be used to estimate the effects of varying raw material characteristics on the final product's mechanical properties, thereby reducing fabrication and testing costs. It could also be extended to analyze specific product applications such as connection details. As such, there is a strong and urgent need for these models in the composite wood industry.

Surprisingly, to date, relatively little research has been conducted on modeling of wood composites. An early study by Hunt and Suddarth (1974) predicted tensile modulus of elasticity and shear modulus of medium-density homogeneous flakeboard using a linear elastic finite-element analysis together with Monte Carlo technique. The model underestimated the experimental tensile modulus by 8% for aspen and 6% for douglas fir, whereas the shear modulus was overestimated by 10% and 13% for aspen and douglas fir, respectively. More recently, Triche and Hunt (1993) developed a linear elastic finite-element model capable of predicting the tensile strength and stiffness of a parallel aligned wood strand composite with controlled geometry. The model was micromechanical in nature, considering each strand to have three layers (i.e., pure wood, resin, and an interface) and the properties of the individual constituents were used as input. Excellent accuracy for the predicted modulus of elasticity was reported (from 0.0% to 11.1% error). However, prediction of maximum stress was inconsistent and in at least one case unacceptable (from 1.2% to 101.1% error). Cha and Pearson (1994) developed a two-

dimensional (2D) finite-element model to predict the elastic tensile properties of a three-ply veneer laminate, consisting of an off-axis core ply of varying angles. Good agreement was obtained between predicted and experimental strains at maximum load (maximum difference of 14.3%) as well as predicted and experimental stresses (maximum difference of 7.7%). Recently, Wang and Lam (1998) developed a three-dimensional (3D), nonlinear, stochastic finite-element model to estimate the probabilistic distribution of the tensile strength of parallel aligned wood strand composites. The model was based fundamentally upon longitudinal tensile strength and stiffness data of individual strands. The model was verified through comparison of predicted and experimental data for four- and six-ply laminates. In all cases, excellent agreement was reported.

It is of interest to note that for all preceding research, save Wang and Lam (1998), focus was placed on linear elastic constitutive theory. Although this may suffice for wood in pure tension, for compression—where the stress-strain behavior is distinctly nonlinear (Goodman and Bodig 1971; Maghsood et al. 1973)—a nonlinear analysis is necessary. For example, restriction of a SCL bending analysis to the elastic range could result in an inefficient design because of the analysis' inability to account for the material strength beyond the proportional limit. Thus, a comprehensive model for SCL, capable of predicting all loading scenarios, must be able to represent both linear and nonlinear behavioral regimes.

To this end, a continuum mechanics approach is adopted herein to model the nonlinear behavior of laminated wood composites up to and including ultimate failure. A materially nonlinear finite-element code has been developed where the nonlinear constitutive behavior of the wood strands is characterized by rate-independent theory of orthotropic plasticity. Also, to account for inherent material variability, the code has extended capacity to perform Monte Carlo simulations.

This research is the preliminary stage of a larger project to develop a computational model to ultimately predict the nonlinear bending behavior of parallel aligned wood strand composites. This material is a simplified version (with convenient and controllable geometry) of the more complex commercial wood composite material, PSL, which contains many strength-reducing characteristics such as voids, overlaps and angle-to-grain deviations. The present study addresses only angle-to-grain deviations. The model is currently formulated to predict the nonlinear load-displacement behavior of symmetric angle-ply laminates, as depicted in Fig. 1.

## MODEL DEVELOPMENT

The model can best be explained with reference to an idealized uniaxial stress-strain curve, as illustrated in Fig. 2. As

<sup>1</sup>PhD Candidate, Dept. of Wood Sci., Univ. of British Columbia, FSC 4041-2424 Main Mall, Vancouver, BC, Canada V6T 1Z4. E-mail: pclousto@interchange.ubc.ca

<sup>2</sup>Assoc. Prof., Dept. of Wood Sci., Univ. of British Columbia, FSC 4041-2424 Main Mall, Vancouver, BC, Canada V6T 1Z4. E-mail: franklam@interchange.ubc.ca

Note. Associate Editor: Arup Maji. Discussion open until January 1, 2002. To extend the closing date one month, a written request must be filed with the ASCE Manager of Journals. The manuscript for this paper was submitted for review and possible publication on May 31, 2000; revised February 13, 2001. This paper is part of the *Journal of Engineering Mechanics*, Vol. 127, No. 8, August, 2001. ©ASCE, ISSN 0733-9399/01/0008-0844-0851/\$8.00 + \$.50 per page. Paper No. 22345.

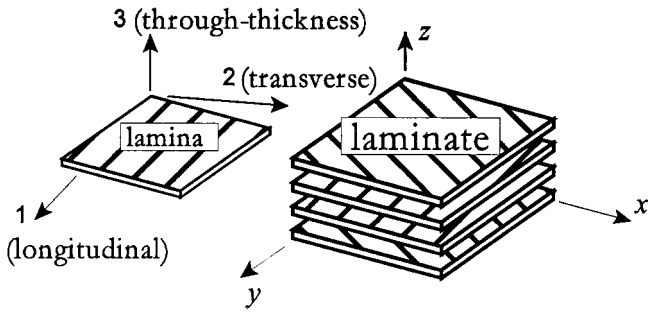


FIG. 1. Angle-Ply Lamina/Laminate and Respective Coordinate Systems

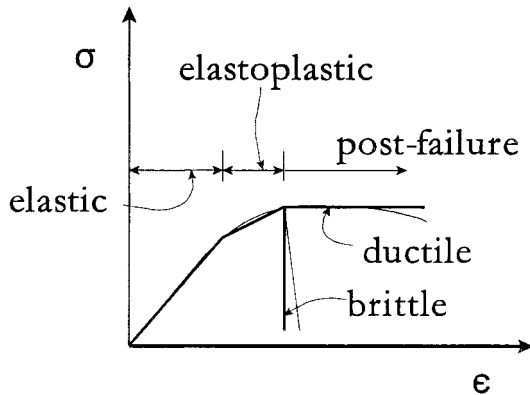


FIG. 2. Idealized Stress-Strain Behavior

shown, the model is comprised of four basic constitutive regimes: elastic, elastoplastic, postfailure brittle, or postfailure ductile. Beyond the elastic domain the material (i.e., integration point) may either (1) fail in a brittle manner or (2) first strain-harden and then ultimately fail in either a ductile or brittle mode. For ductile failure, the material is assumed to lose all stiffness but retains strength, whereas for brittle failure both stiffness and strength are lost. Strain-hardening is characterized by successive growth of the yield surface using associative flow and isotropic hardening. The yield surface is defined by the Tsai-Wu criterion (Tsai and Wu 1971).

### Tsai-Wu Criterion

Strength criteria are used to estimate the combination of stress components ( $\sigma_i$ ) at any point in a member that causes the onset of material failure (or yielding for ductile behavior). The failure/yield surface for the Tsai-Wu criterion in 3D space is described by the equation

$$F_i \sigma_i + F_{ij} \sigma_i \sigma_j = 1 \quad (1)$$

where  $i, j = 1, 2, \dots, 6$  (repeated indices imply summation), and  $F_i$  and  $F_{ij}$  are second and fourth rank strength tensors, respectively. Under a plane stress assumption,  $\sigma_3, \sigma_4,$  and  $\sigma_5$  are assumed negligible and the  $F_6, F_{16},$  and  $F_{26}$  terms are zero due to material orthotropy. The expanded form of (1) then becomes

$$F_1 \sigma_1 + F_2 \sigma_2 + F_{11} \sigma_1^2 + F_{22} \sigma_2^2 + 2F_{12} \sigma_1 \sigma_2 + F_{66} \sigma_6^2 = 1 \quad (2)$$

The coefficients  $F_1$ – $F_{66}$ , with the exception of  $F_{12}$ , are described in terms of the uniaxial strengths in the principal material directions. For a lamina in plane stress, these are: longitudinal strength in both tension and compression ( $X_t, X_c$ ), transverse strength in both tension and compression ( $Y_t, Y_c$ ) and in-plane shear strength ( $S$ ). Using (2) to individually evaluate each uniaxial strength, and performing some simple math-

ematical manipulation, the strength parameters ( $F_i$  and  $F_{ij}$ ) are found to be

$$F_1 = \frac{1}{X_t} - \frac{1}{X_c}; F_2 = \frac{1}{Y_t} - \frac{1}{Y_c}; F_{11} = \frac{1}{X_t X_c}; F_{22} = \frac{1}{Y_t Y_c}; F_{66} = \frac{1}{S^2} \quad (3)$$

The remaining unknown term of (2)  $F_{12}$  is commonly referred to as the interaction parameter, as it accounts for the interaction between the normal stresses. The parameter  $F_{12}$  is commonly determined experimentally, which is a main distinguishing feature of the Tsai-Wu theory from other strength theories. This contributes to the effectiveness of the theory; however, it also presents some challenges in application. Primarily, as first pointed out by Tsai and Wu (1971), the parameter is extremely sensitive to experimental variations. Slight inaccuracies in strength measurements can lead to large inaccuracies in the value of  $F_{12}$ . Moreover, the magnitude of the term is constrained by the stability bound

$$F_{11} F_{22} - F_{12}^2 \geq 0 \quad (4)$$

to ensure closure of the failure/yield surface. Violation of this condition would imply infinite strength for some stress states, which is physically impossible.

Several researchers have reported unacceptable results for experimentally obtained values of  $F_{12}$  (Pipes and Cole 1973; Suhling et al. 1984; Clouston 1995). The earlier studies prompted others to explore theoretical solutions (Cowin 1979; Liu 1984). Despite all efforts, no standard method to determine  $F_{12}$  has been established. For this study, a probabilistic approach has been adopted.

### Orthotropic Plasticity Formulation

The quadratic criterion for yielding of an orthotropic plastic material is written in general form as

$$f \equiv \bar{\sigma}^2(\sigma_i \alpha_i M_{ij}) - k^2 = 0 \quad (5)$$

where  $\bar{\sigma}$  = effective stress or equivalent stress; and  $k$  = threshold stress which is equal to the size of the yield surface. For the purposes of plastic formulation, the Tsai-Wu criterion is adapted to this general form as follows: The square of the effective stress is conveniently defined as

$$\bar{\sigma}^2 = M_{ij}(\sigma_i - \alpha_i)(\sigma_j - \alpha_j) \quad (6)$$

where the terms  $M_{ij}$  and  $\alpha_i = \{\alpha_1, \alpha_2, 0\}^T$  describe the shape of the yield surface and the surface origin, respectively, so that

$$f \equiv M_{ij}(\sigma_i - \alpha_i)(\sigma_j - \alpha_j) - k^2 = 0 \quad (i, j = 1, 2, 6) \quad (7)$$

Expanding this and setting the equalities

$$L_i = 2M_{ij}\alpha_j; K = -M_{ij}\alpha_i\alpha_j + k^2 \quad (8)$$

one obtains

$$f \equiv M_{ij}\sigma_i\sigma_j - L_i\sigma_i - K = 0 \quad (9)$$

Comparing (9) with (2) it can be concluded that

$$M_{ij} \equiv KF_{ij} = K \begin{bmatrix} F_{11} & F_{12} & 0 \\ F_{12} & F_{22} & 0 \\ \text{sym} & & F_{66} \end{bmatrix}; L_i \equiv -KF_i = -K \begin{Bmatrix} F_1 \\ F_2 \\ 0 \end{Bmatrix} \quad (10)$$

It can be noted that the components of  $M_{ij}$  are not independent. For example, if  $M_{11} = 1$  then  $K = 1/F_{11}$  and  $M_{12} = F_{12}/F_{11}$ , etc. (Shih and Lee 1978). Furthermore,  $\alpha_i$  can be found by solving the simultaneous equations

$$L_i = -KF_i = 2M_{ij}\alpha_j = 2KF_{ij}\alpha_j; \text{i.e., } F_i = -2F_{ij}\alpha_j \quad (11)$$

and finally, the square of the threshold stress is calculated as  $k^2 = K + M_{ij}\alpha_i, \alpha_j$ .

### Subsequent Yield Surfaces

The progressive development of the yield surface, in the elastoplastic domain, is handled with subsequent yield surfaces

$$f \equiv \bar{\sigma}^2(\sigma_i, \alpha_i, M_{ij}(\bar{\epsilon}^p)) - k^2(\bar{\epsilon}^p) = 0 \quad (12)$$

where now,  $M_{ij}$  and  $k$  are functions of a hardening parameter, taken in this study to be the effective plastic strain,  $\bar{\epsilon}^p$ . This quantity is derived through association with the plastic work increment by:

$$dW^p = k d\bar{\epsilon}^p = \sigma_i d\epsilon_i^p \quad (13)$$

In deriving the relationship between  $k$  and  $\bar{\epsilon}^p$ , we assume a one-to-one relationship,  $k = H(\bar{\epsilon}^p)$ , which upon differentiation becomes  $dk/d\bar{\epsilon}^p = H'$ .  $H'$ , termed the hardening parameter, can be found from a uniaxial stress-strain test through the formula:

$$H' = E'/(1 - E'/E) \quad (14)$$

where  $E$  = elastic modulus and  $E'$  = slope of the elastoplastic portion of the stress-strain curve.  $H'$  is associated with the expansion of the yield surface and we have, assuming a bilinear stress-strain curve

$$k = k_o + H'\bar{\epsilon}^p \quad (15)$$

where  $k_o$  = initial size of the yield surface.

The strength parameter terms  $M_{ij}$  also vary with plastic deformation. Following a procedure initially proposed by Whang (1969), the nonlinear strength parameters  $X_c$  and  $Y_c$  are updated upon detection of yielding. The updated values are calculated by equating the work done during plastic deformation in a uniaxial test to that produced by the effective stress and effective plastic strain. The resulting updated values are found to be (Whang 1969; Vaziri et al. 1991):

$$X_c^2 = \frac{E_{p1}}{H'}(k^2 - k_o^2) + X_{co}^2; Y_c^2 = \frac{E_{p2}}{H'}(k^2 - k_o^2) + Y_{co}^2 \quad (16)$$

where  $E_{p1}$  and  $E_{p2}$  = hardening parameters for the respective uniaxial stress/strain curves and the subscript "o" refers to the initial yield value.

### Compression versus Tension Dominance

The foregoing plasticity formulation is used to describe strain hardening of the material in the case of a compression-dominant stress state. However, as it is accepted that tensile failure for wood is generally brittle (Barrett et al. 1975; Madson and Buchanan 1986; Barrett et al. 1995), if the stress-state at the failed/yielded location is deemed tension-dominant, brittle failure ensues. The decision between compression or tension dominance is made depending on the combination of stresses at the point of failure. Let us define:  $\gamma_1 = M_{11}(\sigma_1^2 - 2\sigma_1\alpha_1 + \alpha_1^2)$  and  $\gamma_2 = M_{22}(\sigma_2^2 - 2\sigma_2\alpha_2 + \alpha_2^2)$  as portions of the effective stress, which reflect the magnitude of  $\sigma_1$  and  $\sigma_2$ , respectively. Albeit subjective, the stresses at an integration point is deemed tension-dominant, and thereby brittle, when the failure criterion is violated and any one of the following happens: (1)  $\sigma_1 \geq X_t$ ; (2)  $\sigma_2 \geq Y_t$ ; (3)  $\sigma_6 \geq S$ ; (4)  $\sigma_1 \geq 0$  and  $\gamma_1 \geq \gamma_2$ ; or (5)  $\sigma_2 \geq 0$  and  $\gamma_2 \geq \gamma_1$ . The latter two criteria are included to address the case of: (1) large longitudinal tension combined with large shear and (2) large longitudinal compression combined with transverse tension. All other cases of failure are considered ductile.

### Postfailure Modeling

Referencing Fig. 2, when ductile failure occurs, the yield quantities,  $X_c$  and  $Y_c$ , have reached their ultimate values and

the stress level remains constant. When brittle failure occurs, however, the stress level is reduced gradually to facilitate convergence of the iterative procedure. Upon the first iteration of each load increment following brittle failure, the stresses at the failed integration point are reduced to 70, 90, 95, and 98% of the previous value, for  $\sigma_1$  (when tensile),  $\sigma_2$ ,  $\sigma_6$ , and  $\sigma_1$  (when compressive), respectively. These values were derived empirically and provide good postpeak results.

### Constitutive Equations

The constitutive behavior of the layers is defined using the incremental form of Hooke's law to incorporate material non-linearity as

$$\{d\sigma'\}_l = [Q']_l \{d\epsilon'\} \quad (17)$$

where  $l$  refers to the  $l$ th layer of the laminate;  $\{d\sigma'\}_l = \{d\sigma_x, d\sigma_y, d\tau_{xy}\}_l^T$ ,  $\{d\epsilon'\} = \{d\epsilon_x, d\epsilon_y, d\gamma_{xy}\}^T$ , which is the laminate strain increment vector—the same for each layer assuming perfect bonding between layers, and  $[Q']_l$  is the constitutive matrix be it elastic, elastoplastic, or postfailure, depending on the stress level. Primes denote that values have been transformed from ply coordinates (1, 2) to laminate coordinates ( $x, y$ ) (reference Fig. 1). The individual layer constitutive equations are then superimposed using classical lamination to yield the force-strain properties of the laminate:

$$\{dN\} = \sum_{l=1}^n [Q']_l t_l \{d\epsilon'\} \quad (18)$$

where  $\{dN\} = \{N_x, N_y, N_{xy}\}^T$  = vector of resultant in-plane forces acting on the laminate;  $t_l$  = thickness of the  $l$ th layer; and  $n$  = total number of layers.

### Finite-Element Model

A nonlinear, stochastic finite-element code has been developed to incorporate the foregoing constitutive model. The program was used to simulate the load-displacement behavior of symmetric angle-ply laminates using the finite-element mesh as depicted in Fig. 3. The elements (i.e., plane, bilinear, isoparametric elements) are comprised of four layers representing the strands. For each layer, a two-point Gauss quadrature rule was used resulting in 16 stress points per element. The laminate was loaded by prescribing an increasing value of displacement at the five end nodes, as shown. For each increment in displacement, the nonlinearities in the equilibrium equations are resolved using a modified Newton-Raphson iterative procedure. As the structural stiffness becomes either zero or negative beyond the peak load, the initial stiffness is maintained throughout the entire analysis. For each stress point, within each iteration, the stresses were monitored for failure or yield in accordance with (7) or (12), depending on stage of plasticity.

### Model Limitations

It is noted that in using simple planar elements, the model assumes that interlaminar stresses associated with the through-

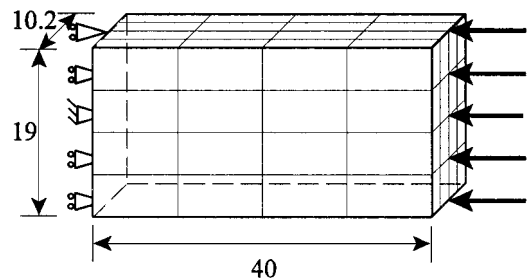


FIG. 3. Finite-Element Representation

thickness ( $z$ ) direction are negligible. This is a valid assumption if (1) the laminate is symmetric, (2) the applied loads on the laminate are statically equivalent to in-plane forces producing neither bending nor twisting, and (3) “free-edge” effects are negligible. The present study complies with the first two criteria. The third criteria leads to a phenomenon known as delamination, which has been extensively studied both theoretically and experimentally for many advanced composite materials (Pipes and Pagano 1971; Whitney and Browning 1972; Gibson 1994). These studies show that within a “boundary region” (roughly one laminate thickness inward from the free edge of the laminate), a 3D stress state exists. Although this must be true for the present wood specimens, no delamination was witnessed during testing. This is likely because failure was instead governed either by perpendicular to grain tensile stresses or by in-plane shear stresses. It would be advised that for future studies dealing with more complex, non-symmetric composite beams, neglecting out-of-plane stresses could lead to significant errors.

## EXPERIMENTAL DATABASE

### Laminae Properties

Evident from the failure criterion, the model requires as input the principal properties (tensile, compressive, and shear strength, and stiffness) of the individual layers. Tests were performed on coastal douglas-fir strands that were air dried to a moisture content of 4–9%. Tensile tests were conducted at the University of British Columbia. A 250 kN material test machine (MTS) machine with mechanical wedge-action grips as well as a 25.4 mm gauge length extensometer was used as depicted in Fig. 4—the results of which are summarized in Table 1. The longitudinal specimens were individual strands whereas the transverse specimens, to avoid breakage during handling, were small laminates consisting of six strands each. The tensile properties (both parallel and perpendicular to the

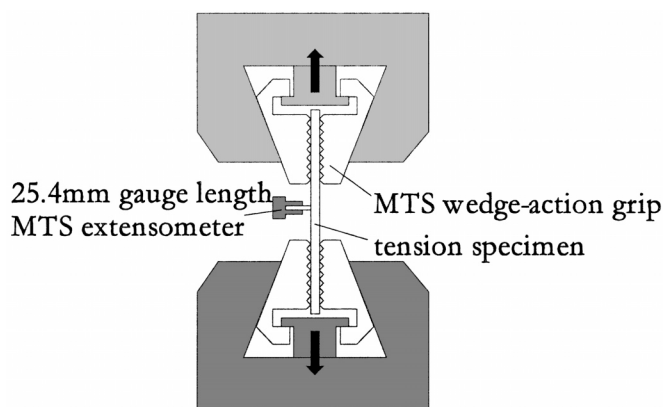


FIG. 4. Tension Test Setup

grain) are assumed linear elastic and are thus defined by two variables each:  $E_{1T}$ ,  $X_T$ , and  $E_{2T}$ ,  $Y_T$ —elastic modulus and ultimate strength in the parallel and perpendicular direction, respectively.

Compression tests were conducted at l’Ecole Normale Supérieure (ENS), Cachan, France. Swivel bearings, both top and bottom, were used to prevent eccentric loading on the specimen as shown in Fig. 5. Stiffness moduli were determined using the cross-head displacement. Results are summarized in Table 1. The compressive properties are nonlinear and consequently require more variables to describe their mechanical behavior. From Fig. 6, the stress-strain curve for parallel to grain compression, for example, has been simplified to a trilinear approximation and can be defined using four variables:  $E_{1C}$ ,  $X_C$ ,  $E'_{1C}$ , and  $X_C^u$ , which denote the elastic modulus prior to yielding, the yield stress, the elastoplastic tangent modulus beyond yield, and the ultimate stress, respectively. These val-

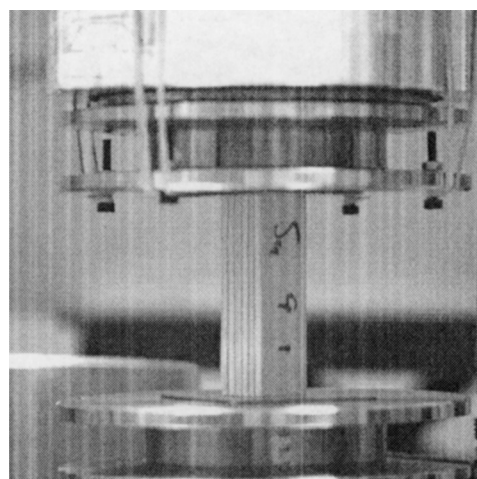


FIG. 5. Compression Test Setup

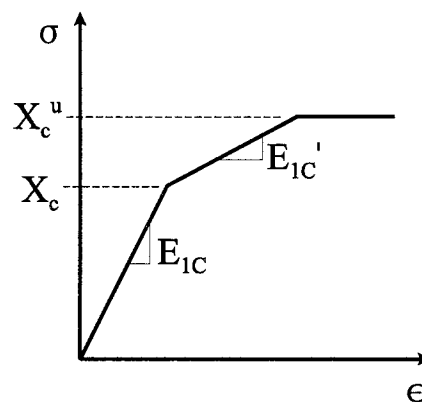


FIG. 6. Trilinear Approximation of Compressive Stress-Strain Behavior

TABLE 1. Tension and Compression Database for Laminae

Test	Nominal dimension (mm <sup>3</sup> )	Count	PROPERTY							
			Elastic Stiffness		Proportional Limit		Tangent Stiffness		Ultimate Stress	
			Average (GPa)	COV (%)	Average (MPa)	COV (%)	Average (GPa)	COV (%)	Average (MPa)	COV (%)
Longitudinal compression	17 × 19 × 40	53	10.09	19.13	67.32	8.04	1.93	33.11	76.46	7.06
Transverse compression	17 × 19 × 40	54	0.49	15.23	15.37	11.75	0.11	35.05	18.19	9.28
Longitudinal tension	3 × 19 × 51	36	15.46	30.50	—	—	—	—	68.77	26.68
Transverse tension	17 × 19 × 150	45	0.09	24.40	—	—	—	—	1.91	18.31

ues were determined for each specimen by equating the area under the experimental stress-strain curve (i.e., the strain energy stored in the specimen) to the area of the fitted trilinear stress-strain curve. Perfect plasticity beyond ultimate load (as opposed to strain softening) has been assumed. This assumption not only simplifies the analysis greatly, but also agrees with experimental results (up to an acceptable strain level).

It is noted here that the tensile strengths given in Table 1 reflect only the strength of the corresponding tested volume. Prior to implementing the values into the finite element code, adjustments must first be made for size. This size effect is most prominent with brittle modes of failure and is dependent on the strength variability of the material. Size effect has been acknowledged and addressed in many wood and timber studies, such as Barrett et al. (1975), Madsen and Buchanan (1986), and Barrett et al. (1995), as well as SCL studies by Sharp and Suddarth (1991) and Clouston et al. (1998). Each of these studies espoused the use of Weibull weakest-link theory to quantify size effect. As such, this theory was adopted for this study. Transverse tension strength was adjusted from representing that of the tested volume to that of the tributary area for one Gauss point. Longitudinal strength was adjusted however, from the experimental gauge length to the simulated model gauge length. In all cases, the relationship

$$\frac{\tau_1}{\tau_2} = \left(\frac{V_2}{V_1}\right)^{1/\beta} \quad (19)$$

was used, where the strengths  $\tau_1$  and  $\tau_2$  correspond to the volumes  $V_1$  and  $V_2$ , respectively, and  $\beta$  is the shape parameter of the two-parameter Weibull distribution for that test configuration. (Clouston et al. 1998).

Because the analysis is stochastic, the strengths and stiffnesses for each layer are represented by appropriate probability distributions. The tensile properties are randomly generated lognormal values. The compressive properties, however, are generated in accordance with a bivariate standard normal distribution, as follows:

$$b_i = \mu_{bi} + \sum_{j=1}^4 C_{ij}z_j \quad (i = 1, 2, 3, 4) \quad (20)$$

where (for parallel to grain properties, for example)  $b_1 = E_{1c}$ ;  $b_2 = X_c$ ;  $b_3 = E'_{1c}$ ;  $b_4 = X_c''$ ;  $\mu_{bi}$  = respective variable mean;  $C_{ij}$  = lower triangle of the correlation matrix of the variables, derived through Cholesky decomposition; and  $z_i$  = an independent standard normal random variable. The experimental results are very well represented by the simulated values, as illustrated in Fig. 7.

All strength and stiffness properties were assumed to vary

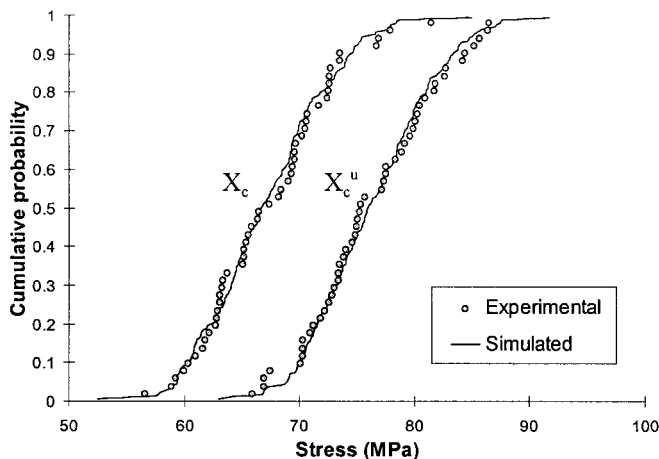


FIG. 7. Cumulative Probability Distribution for  $X_c$  and  $X_c''$

between layers, with the exception of tension perpendicular to grain strength, which was instead regenerated for each integration point. This strength was treated differently because in addition to yielding good results, material behavior in this configuration is believed to be more in keeping with ideal brittle fracture theory. In this configuration, the within-member variation is less likely to be correlated as it is, for example, for tension parallel to grain (Lam and Varoglu 1990). The failure mechanism is more likely perfectly brittle, failing completely when fracture occurs at the weakest point. The material flaws are assumed to be randomly distributed.

### In-Plane Shear Strength ( $S$ ), Shear Modulus ( $G$ ), and Interaction Parameter ( $F_{12}$ )

Various approaches have been taken in the past to evaluate the shear properties of wood, the most popular being the ASTM shear block method for small clear specimens as described in ASTM D 143-99. This method, however, produces a complex stress distribution in the specimen, and hence, a questionable estimation of pure shear strength. An added challenge lays in finding the pure shear characteristics of a wood strand (i.e., practical difficulties in testing the strand due to its geometry). Furthermore, there are complications, as outlined previously, with establishing the interaction parameter of the Tsai-Wu criterion. As such, an alternative method to evaluating these three variables [shear strength ( $S$ ), shear modulus ( $G$ ), and interaction parameter ( $F_{12}$ )] has been developed as given next.

The variables are obtained simultaneously through a nonlinear least-square minimization of error approach between the predicted and experimental compression strengths of a  $[\pm 15]_s$  angle-ply laminate. Tests were conducted on the laminate (nominal dimensions:  $11 \times 19 \times 40 \text{ mm}^3$ ) at ENS, Cachan, France. The descriptive statistics for the results are given in both Table 2 and Fig. 8.

In short, the procedure entailed minimizing the function

$$\Phi = \sum_{i=1}^p \left(1 - \frac{\tau_i^{\text{pred}}}{\tau_i^{\text{exp}}}\right)^2 \quad (21)$$

TABLE 2. Results of Nonlinear Minimization

Statistics	[ $\pm 15$ ] <sub>s</sub> Compression				
	Experimental	Simulated	$S$	$G$	$F_{12}$
Average (MPa)	51.57	51.65	5.99	232.77	5.14E-04 MPa <sup>-2</sup>
COV (%)	14.42	15.39	11.73	17.76	71.73

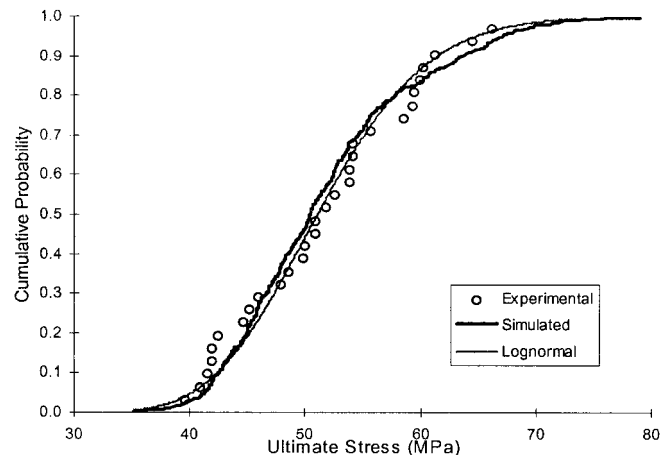


FIG. 8. Cumulative Probability Distribution of  $[\pm 15]_s$  Laminate in Compression

with respect to the mean and standard deviation of each of the three variables ( $S$ ,  $G$ ,  $F_{12}$ ), where  $P$  denotes the number of probability levels for consideration and the superscripts “pred” and “exp” refer to the predicted and experimental laminate strengths, respectively. The compressive strengths of the laminates were simulated using the finite element analysis, in conjunction with a Monte Carlo simulation routine to produce the probabilistic distributions. Strength was first calculated based on initial estimates for the mean and standard deviation of the three variables. This predicted strength was ranked (i.e., sorted in ascending order and given the associated probability of failure). The residual function  $\Phi$  was then calculated, where the predicted strength was determined for the same  $i$ th probability level as the experimental strength.

Based on the gradient of the residual function, estimated by a perturbation process, adjusted values of the mean and standard deviation of the three variables were computed. These new, adjusted, statistical parameters replaced the initial estimated values and the residual function was re-evaluated. This procedure was repeated until the difference between residual function values for subsequent iterations satisfied a set tolerance of  $1.0 \times 10^{-3}$ .

Referring to Table 2, the average values and variability obtained for  $S$ ,  $G$ , and  $F_{12}$  appear reasonable. Shear and shear modulus for Douglas fir clear wood have been reported by Bodig and Jayne (1993) as 6.4 MPa and approximately (using a 14:1 ratio for  $E_1:G$ ) 800 GPa. The difference between the calculated and published results for the latter is attributed to the thin nature of strands as opposed to solid wood specimens. The interaction parameter  $F_{12}$  is more difficult to evaluate as there is no directly comparable data in the literature for wood strands. As such, one can evaluate it based on its conformity to a deterministic evaluation of the stability bounds [(4)]. Using the deterministic average values of the strength parameters from Table 1 and adjusting the tensile strengths for size effect, the bounds were found to be  $\pm 1.51 \times 10^{-3} \text{ MPa}^{-2}$ . The result of  $5.14 \times 10^{-4} \text{ MPa}^{-2}$  falls within these bounds however, the coefficient of variation is quite high: 71.73%. This is likely a consequence of the parameter’s high sensitivity to experimental variation.

The model predicts the average ultimate compression strength of a  $[\pm 15]_s$  angle-ply laminate to be 51.65 MPa. This is very close to the experimental result, 51.57 MPa, as would be expected since the parameters were fitted using this experimental data. The predicted variability is also very accurate, with predicted and experimental coefficients of variations of 15.4% and 14.4%, respectively. Fig. 8 illustrates these results visually through a comparison of the experimental and simulated cumulative probability distributions. Also, for reference, a lognormal distribution was plotted. Comparing the three curves, the experimental data tends to deviate slightly at the lower end of the curve, possibly due to manufacturing or test imperfections. Overall, however, the model predictions fit the experimental data extremely well.

## MODEL VERIFICATION

The computer model, now in a complete state, was used to predict the strength of other test configurations made from the

same material:  $[\pm 15]_s$  laminates in tension and  $[\pm 30]_s$  laminates in both tension and compression. Laminates were fabricated and tested for comparison. All laminates were nominally  $19 \times 10.5 \text{ mm}^2$  in cross section. The laminates tested in compression were nominally 40 mm long to comply with the requirements of ASTM D 198-99 for short columns with no lateral support. The  $[\pm 15]_s$  tensile specimens were 120 mm long and the  $[\pm 30]_s$  laminates 60 mm long. A longer test length was used for  $[\pm 15]_s$  laminates to ensure wood fibres were not continuous from one test grip to the other, potentially increasing observed strength.

The results of both numerical simulations and experiments are summarized in Table 3 and Figs. 9–11. As evident from Table 3, the average value of the ultimate strengths (maximum percent error of 3.99%) and corresponding coefficient of variations (predicted range from 9.6 to 20.7%; test data range from 9.0 to 16.6%) are well predicted. The cumulative probability distributions in Figs. 9–11 offer a visual comparison of the predicted and experimental results.

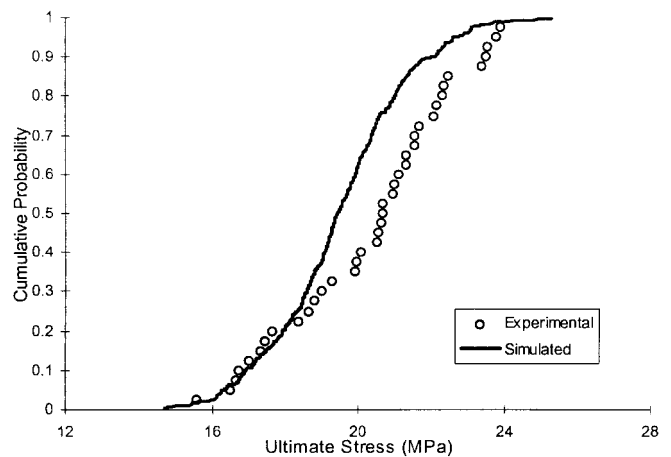


FIG. 9. Cumulative Probability Distribution of  $[\pm 30]_s$  Laminate in Compression

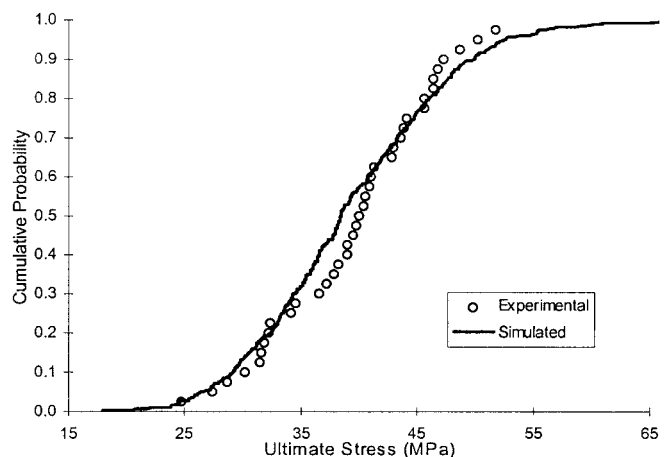


FIG. 10. Cumulative Probability Distribution of  $[\pm 15]_s$  Laminate in Tension

TABLE 3. Results of Experimental and Simulated Tests

Statistics	$[\pm 15]_s$			$[\pm 30]_s$					
	Tension		Error (%)	Tension			Compression		
	Experimental	Simulated		Experimental	Simulated	Error (%)	Experimental	Simulated	Error (%)
Average (MPa)	39.38	39.14	0.61	21.71	21.32	1.80	20.30	19.49	3.99
COV (%)	16.72	20.72	23.92	9.01	12.12	34.52	11.12	9.57	13.94

To further demonstrate the applications of the computer model, 500 stress-strain curves for the  $[\pm 15]_s$  and  $[\pm 30]_s$  compression laminates were computer generated and compared with the actual experimental curves. The tensile results were not comparable in this case due to the experimental test setup. Here the MTS tension grips used were of a wedge type such that as the load increased, the measured displacement of the specimen included inherent displacement within the grips thereby producing an erroneous load-displacement curve. Any test requiring accurate load displacement curves (i.e., longitudinal or transverse tests for modulus-of-elasticity calcula-

tion) were conducted with an MTS extensometer mounted on the specimen. The results showing the load increments for the compression specimens are given in Figs. 12 and 13. For clarity, only five curves of each (experimental and simulated) have been shown, which represent the approximate average as well as the upper and lower bound for both stiffness and strength. The experimental results have been zero-adjusted to remove nonlinearities at the curve origin. This was done by shifting the curve in the  $x$ -direction only, such that the projection of the linear portion of the load-displacement curve passes through the origin. The nonlinearities occur due to the settling of the specimen within the rotating spherical bearing blocks, used to prevent eccentric loading on the specimen.

The simulated curves clearly lay within the experimental bounds. The diagrams also demonstrate that the  $[\pm 15]_s$  laminates tend to behave more plastically, since for this configuration compressive parallel to grain stresses govern, whereas for the  $[\pm 30]_s$  laminates, tensile perpendicular to grain stresses govern, resulting in a more brittle laminate behavior.

## CONCLUSION

The foregoing numerical simulations demonstrate the use of a plasticity based stochastic finite-element model to predict the fundamental material response of  $[\pm 15]_s$  and  $[\pm 30]_s$  angle-ply laminates. Moreover, a unique method has been described to evaluate the shear characteristics and the interaction parameter of the Tsai-Wu theory of a wood strand laminae. It is important to note that the model is, at present, accurate for only the configurations considered. Further validation of the model is necessary for other modes and configurations. The practical significance of the present results is that orthotropic plasticity theory, in conjunction with stochastic analysis, appears to be a very promising technique in modeling the nonlinearities in the stress-strain behavior of wood strand composites.

## ACKNOWLEDGMENTS

Gratitude is extended to Trus Joist Macmillan Ltd., Weyerhaeuser Ltd., and NSERC Canada (FSP 0166869) for providing funding for the project. As well, l'Ecole Normale Supérieure (ENS)—Laboratoire de Mécanique et Technologie—Cachan, France are acknowledged for providing facilities for the compression tests.

## REFERENCES

- ASTM. (1999). "Standard methods of testing small clear specimens of timber." *D 143*, West Conshohoken, Pa.
- ASTM. (1999). "Standard methods of testing static tests of timbers in structural sizes." *D 198*, West Conshohoken, Pa.
- Barrett, J. D., Foschi, R. O., and Fox, S. P. (1975). "Perpendicular-to-grain strength of douglas-fir." *Can. J. Civ. Engrg.*, 2(1), 50–57.
- Barrett, J. D., Lam, F., and Lau, W. (1995). "Size effects in visually graded softwood structural lumber." *J. Mat. in Civ. Engrg.*, 7(1), 19–30.
- Bodig, J., and Jayne, B. A. (1993). *Mechanics of wood and wood composites*, Krieger, Malabar, Fla.
- Cha, J. K., and Pearson, R. G. (1994). "Stress analysis and prediction in 3-layer laminated veneer lumber: Response to crack and grain angle." *Wood and Fiber Sci.*, 26(1), 97–106.
- Clouston, P. (1995). "The Tsai-Wu strength theory for douglas-fir laminated veneer." MSc thesis, University of British Columbia, Vancouver.
- Clouston, P., Lam, F., and Barrett, J. D. (1998). "Incorporating size effects in the Tsai-Wu strength theory for douglas-fir laminated veneer." *Wood Sci. and Technol.*, 32(3), 215–226.
- Cowin, S. C. (1979). "On the strength anisotropy of bone and wood." *ASME Trans., J. Appl. Mech.*, 46(4), 832–837.
- Gibson, R. F. (1994). *Principles of composite material mechanics*, McGraw-Hill, New York.
- Goodman, J. R., and Bodig, J. (1971). "Orthotropic strength of wood in compression." *Wood Sci.*, 4(2), 83–94.
- Hunt, M. O., and Suddarth, S. K. (1974). "Prediction of elastic constants of particleboard." *Forest Products J.*, 24(5), 52–57.
- Lam, F., and Varoglu, E. (1990). "Effect of length on the tensile strength of lumber." *Forest Products J.*, 40(5), 37–42.

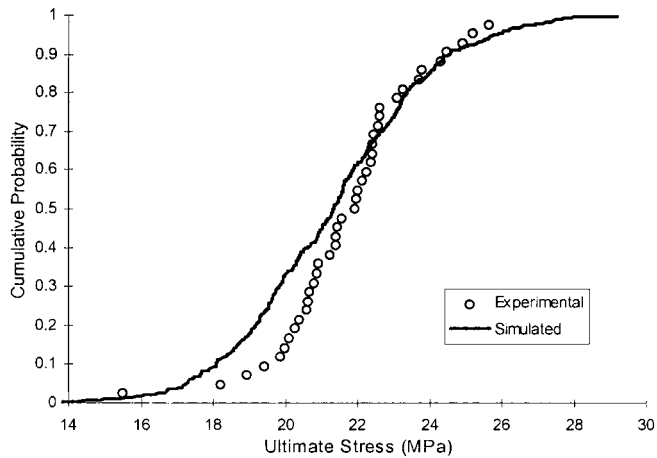


FIG. 11. Cumulative Probability Distribution of  $[\pm 30]_s$  Laminate in Tension

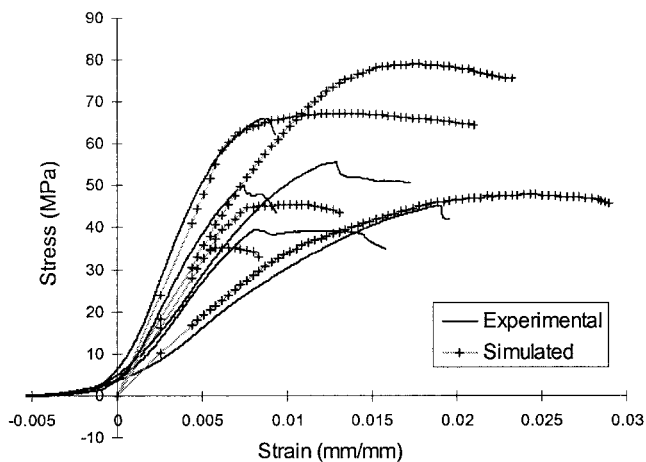


FIG. 12. Stress/Strain Curves for  $[\pm 15]_s$  Laminate in Compression

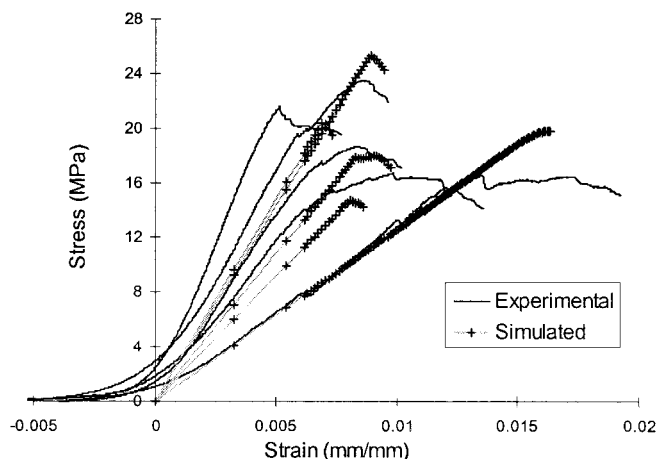


FIG. 13. Stress/Strain Curves for  $[\pm 30]_s$  Laminate in Compression

- Liu, J. Y. (1984). "Evaluation of the Tensor Polynomial Strength Theory for Wood." *J. Compos. Mat.*, 18(1), 216–225.
- Madsen, B., and Buchanan, A. H. (1986). "Size effects in timber explained by a modified weakest-link theory." *Can. J. Civ. Engrg.*, 13(2), 218–232.
- Maghsood, J., Scott, N. R., Furry, R. B., and Sexsmith, R. (1973). "Linear and nonlinear finite element analysis of wood structural members." *ASAE Trans.*, Paper No. 70-922, 490–496.
- Pipes, R. B., and Cole, B. W. (1973). "On the off-axis strength test for anisotropic materials." *J. Compos. Mat.*, 7(1), 246–256.
- Pipes, R. B., and Pagano, N. J. (1971). "Interlaminar stresses in composite laminates under uniform axial extension." *J. Compos. Mat.*, 4(1), 538–548.
- Sharp, D. J., and Suddarth, S. K. (1991). "Volumetric effects in structural composite lumber." *Proc., Int. Timber Engrg. Conf.*, London, 3, 427–433.
- Shih, C. F., and Lee, D. (1978). "Further developments in anisotropic plasticity." *Trans. ASME, J. Engrg. Mat. and Technol.*, 100(1), 294–302.
- Suhling, J. C., Rowlands, R. E., Johnson, M. W., and Gunderson, D. E. (1984). "Tensorial strength analysis of paperboard." *Experimental Mech.*, 25(1), 75–84.
- Triche, M. H., and Hunt, M. O. (1993). "Modeling of parallel-aligned wood strand composites." *Forest Products J.*, 43(11/12), 33–44.
- Tsai, S. W., and Wu, E. M. (1971). "A general theory of strength for anisotropic materials." *J. Compos. Mat.*, 5(1), 58–80.
- Vaziri, R., Olson, M. D., and Anderson, D. L. (1991). "A plasticity-based constitutive model for fibre-reinforced composite laminates." *J. Compos. Mat.*, 25(5), 512–535.
- Wang, Y. T., and Lam, F. (1998). "Computational modeling of material failure for parallel-aligned strand based wood composites." *Computational Mat. Sci.*, 11(3), 157–165.
- Whang, B. (1969). "Elastic-plastic orthotropic plates and shells." *Proc., Symp. On Application of Finite Element Meth. in Civ. Engrg.*, Vanderbilt University, Nashville, Tenn., 481–515.
- Whitney, J. M., and Browning, C. E. (1972). "Free-edge delamination of tensile coupons." *J. Compos. Mat.*, 6(1), 300–303.

- $C_{ij}$  = lower triangle of correlation matrix;  
 $E$  = elastic modulus;  
 $E'$  = tangent modulus;  
 $F_{ij}, M_{ij}$  = tensors of strength parameters;  
 $G$  = in-plane shear modulus;  
 $H', E_{p1}, E_{p2}$  = hardening parameters;  
 $k$  = threshold stress;  
 $\{N\}$  = resultant in-plane force vector;  
 $n$  = total number of layers;  
 $P$  = number of probability levels;  
 $[Q]_l$  = material stiffness matrix for  $l$ th layer of laminate;  
 $S$  = in-plane shear strength;  
 $t$  = thickness of lamina;  
 $V$  = volume;  
 $W^p$  = plastic work;  
 $X_t$  = longitudinal tensile strength;  
 $X_c, X_c^u$  = longitudinal compressive yield and ultimate strength, respectively;  
 $Y_t$  = transverse tensile strength;  
 $Y_c, Y_c^u$  = transverse compressive yield and ultimate strength, respectively;  
 $z_i$  = standard normal random variable;  
 $\alpha_i$  = parameters which define offset of yield surface;  
 $\beta$  = shape parameter of two-parameter Weibull distribution;  
 $\gamma_i$  = portion of effective stress;  
 $\epsilon_i^p$  = plastic strain components;  
 $\bar{\epsilon}^p$  = effective plastic strain;  
 $\sigma_i$  = stress components;  
 $\bar{\sigma}$  = effective stress;  
 $\tau$  = nonspecific material strength; and  
 $\Phi$  = minimization function.

## NOTATION

The following symbols are used in this paper:

- $b_i$  = randomly generated bivariate standard normal parameter;

## Subscripts

- $x, y, z$  = laminate coordinate directions; and  
 $1, 2, 3$  = principal material directions.